Title

The RhLOL1—RhILR3 module mediates cytokinin-induced petal abscission in rose

Journal

New Phytologist, 237(2)

ISSN

0028-646X

Authors

Jiang, Chuyan

Liang, Yue

Deng, Shuning

et al.

Publication Date

2023

DOI

10.1111/nph.18556

Peer reviewed

New Phytologist

Research

The *Rh*LOL1–*Rh*ILR3 module mediates cytokinin-induced petal abscission in rose

Chuyan Jiang[1], Yue Liang[1], Shuning Deng[1], Yang Liu[1], Haohao Zhao[1], Susu Li[1], Cai-Zhong Jiang[2,3], Junping Gao[1] and Chao Ma[1]

[1]Beijing Key Laboratory of Development and Quality Control of Ornamental Crops, Department of Ornamental Horticulture, College of Horticulture, China Agricultural University, Beijing, 100193, China; [2]Crops Pathology and Genetic Research Unit, United States Department of Agriculture, Agricultural Research Service, Davis, CA 95616, USA; [3]Department of Plant Sciences, University of California at Davis, Davis, CA 95616, USA

Author for correspondence:
Chao Ma
Email: mac@cau.edu.cn

Received: *25 March 2022*
Accepted: *8 October 2022*

New Phytologist (2022)
doi: 10.1111/nph.18556

Key words: abscission, Aux/IAA, auxin, bHLH transcription factor, cytokinin (CK), LSD1, *Rosa hybrida*.

Summary

- In many plant species, petal abscission can be considered the final step of petal senescence. Cytokinins (CKs) are powerful suppressors of petal senescence; however, their role in petal abscission is ambiguous.
- Here, we observed that, in rose (*Rosa hybrida*), biologically active CK is accumulated during petal abscission and acts as an accelerator of the abscission process. Using a combination of reverse genetics, and molecular and biochemical techniques, we explored the roles of a LESION SIMULATING DISEASE1 (LSD1) family member Rh*LOL1* interacting with a bHLH transcription factor *Rh*ILR3 in CK-induced petal abscission.
- Silencing Rh*LOL1* delays rose petal abscission, while the overexpression of its ortholog Sl*LOL1* in tomato (*Solanum lycopersicum*) promotes pedicel abscission, indicating the conserved function of *LOL1* in activating plant floral organ abscission. In addition, we identify a bHLH transcription factor, *Rh*ILR3, that interacts with *Rh*LOL1. We show that *Rh*ILR3 binds to the promoters of the auxin signaling repressor auxin/indole-3-acetic acid (*Aux/IAA*) genes to inhibit their expression; however, the interaction of *Rh*LOL1 with *Rh*ILR3 activates the expression of the *Aux/IAA* genes including Rh*IAA4-1*. Silencing Rh*IAA4-1* delays rose petal abscission.
- Our results thus reveal a *Rh*LOL1–*Rh*ILR3 regulatory module involved in CK-induced petal abscission via the regulation of the expression of the *Aux/IAA* genes.

Introduction

Abscission is a physiological process directly linked to senescence. In the context of senescence, the final phase of a flower's life is one of three types: petal wilting, withering, or the abscission of turgid petals (Woltering & van Doorn, 1988; van Doorn, 2001; Wu *et al.*, 2017; Ma *et al.*, 2021). Petal abscission is therefore considered one of the terminal phases of flower senescence.

Petal senescence and abscission are closely coordinated and precisely regulated by phytohormones. In most cases, hormones have similar effects on petal abscission and senescence (Estornell *et al.*, 2013); for example, ethylene is a critical accelerator of the petal senescence and abscission processes. Exogenous ethylene treatment accelerates petal senescence and abscission in the majority of abscission-prone flowers studied (Woltering & van Doorn, 1988). In *Arabidopsis thaliana*, the ethylene-insensitive mutants *ethylene response1-1* (*etr1-1*) and *ethylene insensitive2-1* (*ein2-1*) exhibited delayed petal senescence and abscission (Lim, 2003; Patterson & Bleecker, 2004; Patharkar & Walker, 2017). Auxin is a pivotal inhibitor of petal abscission and senescence, and its molecular mechanisms in both processes have been well investigated. In the auxin signaling pathway, auxin/indole-3-acetic acid (Aux/IAA) proteins repress the activity of the auxin response factor (ARF) transcription factors by forming heterodimers with them. Auxin promotes the degradation of the Aux/IAAs and subsequently releases the ARFs to activate the downstream genes (Lavy & Estelle, 2016; Leyser, 2018). In Arabidopsis, *ARF1*, *ARF2*, *ARF7*, and *ARF19* function redundantly in organ senescence and petal abscission (Ellis *et al.*, 2005; Okushima *et al.*, 2005).

Previous studies have suggested that cytokinins (CKs) may play differing regulatory roles between organ senescence and abscission. Cytokinin has been widely shown to be a suppressor of flower senescence (Lim, 2003; Wu *et al.*, 2017; Honig *et al.*, 2018). In rose (*Rosa hybrida*), varieties with long flower longevity have higher CK contents in their petals than those with shorter-lived flowers (Mayak & Halevy, 1970). Exogenous CK treatments can delay petal senescence in several plant species, including carnations (*Dianthus caryophyllus*), petunia (*Petunia hybrida*), and rose (Mayak & Halevy, 1970; Eisinger, 1977; Mor *et al.*, 1983; Taverner *et al.*, 1999), and the overexpression of the CK biosynthesis gene *isopentenyltransferase* delayed flower

senescence in petunia (Chang *et al.*, 2003). On the contrary, several studies indicated that CK plays the part of an accelerator in organ abscission (Estornell *et al.*, 2013; Ma *et al.*, 2021). A synthetic CK-like molecule, thidiazuron, has been widely used as a defoliant in agriculture to facilitate mechanical harvesting for many crops, especially cotton (*Gossypium* sp.; Xu *et al.*, 2019). In apple (*Malus domestica*), the application of synthetic CK-like compounds can significantly promote fruitlet abscission (Dal Cin *et al.*, 2007); however, the role of CK in petal abscission is still ambiguous.

LESION SIMULATING DISEASE1 (*LSD1*)-like genes encode a small plant-specific family of zinc finger proteins that contain zinc finger LSD domains: CxxCRxxLMYxxGASxVxCxxC (Dietrich *et al.*, 1997; He *et al.*, 2011; Wituszyńska *et al.*, 2013). In Arabidopsis, functional analyses of *lsd1* mutants demonstrated that *LSD1*-like genes participate in programmed cell death (Torres *et al.*, 2005; Wang *et al.*, 2005; Muhlenbock *et al.*, 2007; Li *et al.*, 2013; Borovsky *et al.*, 2019) and in the responses to abiotic and biotic stresses (Muhlenbock *et al.*, 2008; Wituszyńska *et al.*, 2013; Bernacki *et al.*, 2021). Zinc finger LSD domains have been suggested to be responsible for DNA–protein binding, indicating that LSD1-like proteins might act as transcription factors or scaffold proteins (Czarnocka *et al.*, 2017). To date, however, the molecular basis of LSD1-like protein function is still largely unknown.

Rose is an important ornamental crop world-wide, and its commercial value depends on the longevity of its cut flowers. Here, we report that CK plays a role in accelerating rose petal abscission, and a CK-induced *LSD1*-like gene, Rh*LOL1* (*LSD1-Like1*), accelerates petal abscission. The detailed mechanism by which Rh*LOL1* influences petal abscission is described in this study.

Materials and Methods

Plant materials and treatments

The abscission-prone rose (*Rosa hybrida* L.) cultivar 'Golden Shower' was used for all the experiments except virus-induced gene silencing (VIGS) assays, for which a rose cultivar 'Samantha' with high VIGS efficiency was used. For 'Golden Shower', the plants were grown in a controlled environment room at China Agricultural University (Beijing, China). Their flowers at flower opening stage 2 were harvested and transported to the laboratory within 1 h. For 'Samantha', the plantlets were propagated by tissue culture, as described previously (Wu *et al.*, 2017; Gao *et al.*, 2019).

The rose plantlets, tomato (*Solanum lycopersicum* L. cv MicroTom), and *Nicotiana benthamiana* L. plants were grown in a growth chamber at 23 ± 1°C and 40–60% relative humidity under a 16 h : 8 h, light : dark photoperiod.

For CK treatments, cut rose flowers of 'Golden Shower' at opening stage 2 were placed in vases containing 10 μM N6-(Δ^2-isopentenyl)-adenine (iP; D168889; Aladdin, Shanghai, China) or 100 μM 6-benzyl aminopurine (6-BA, a synthetic CK; B3408; Sigma). Mock samples were placed in 0.1% dimethyl sulfoxide (DMSO). We conducted flower longevity analyses at 23 ± 1°C and 40–60% relative humidity under a 16 h : 8 h, light : dark photoperiod. The phenotype of the flowers was recorded every day.

Quantification of endogenous CK levels

About 120 mg of rose petal abscission zone (AZ) tissues at different opening stages was frozen and ground to powder. The powders were extracted with 80% methanol overnight at 4°C. The CK contents were detected by MetWare (http://www.metware.cn/) using the QTrap4500 liquid chromatography–mass spectrometry (LC–MS)/MS platform (AB Sciex, Framingham, MA, USA). Three biological replicates were performed for each sample.

Immunolocalization of iP

Petal AZs were harvested from flowers at different stages. The samples were fixed in 4% (w/v) paraformaldehyde and 1% (v/v) glutaraldehyde using vacuum infiltration, and shaken overnight at 4°C. The samples were dehydrated using a gradient series of ethanol solutions (30%, 50%, 70%, 80%, 95%, and 100% twice, v/v) for 1 h each time at room temperature and then were infiltrated with xylene and paraplast. After 3 d of wax infiltration, the samples were embedded in paraplast and cut into 10-μm-thick sections using a microtome (HistoCore Biocut; Leica Biosystems, Wetzlar, Germany). The specimens were incubated in a blocking solution containing 10% sheep serum and 25 mg ml^{-1} BSA, were incubated with N6-isopentenyladenosine antibody (AS09435; Agrisera, Vännäs, Sweden; Dewitte *et al.*, 1999) at 37°C for 2 h, sequentially incubated with anti-Rabbit IgG-Gold antibody (G7402; Millipore Sigma, Darmstadt, Germany) at 37°C for 1 h, and stained with developing solution. The negative controls were specimens not incubated with the N6-isopentenyladenosine antibody.

RNA extraction, RT-qPCR, and RNA-seq analyses

Tissues (petal, petal AZ, and receptacle) were harvested and frozen in liquid nitrogen, and total RNA was extracted using the hot borate method as described previously (Liang *et al.*, 2020).

For the reverse transcription polymerase chain reaction (RT-qPCR), 1 μg of DNase-treated RNA was used to synthesize the first-strand cDNA using oligo d(T) and random primers in a final volume of 20 μl. The 20-μl RT-qPCRs were performed using 1 μl cDNA as the template and a Step One Plus real-time PCR system (Thermo Fisher Scientific, Waltham, MA, USA) in standard mode using the KAPA SYBR FAST quantitative PCR kit (Roche). Rh*UBI2* was used as the internal control (Liang *et al.*, 2020). Each experiment was performed independently three times. The primers used in this study are listed in Supporting Information Table S1.

For the RNA-seq analysis, three biological replicates of petal AZs at stage 5 in TRV and Rh*LOL1*-silenced plants were collected and extracted RNA. The RNA integrity was analyzed using an Agilent RNA Nano 6000 Assay Kit on an Agilent 2100 bioanalyzer (Agilent Technologies, Palo Alto, CA, USA). The qualified RNA sample was sent to Beijing Novogene Bioinformatics Technology Co. Ltd

(http://www.novogene.com/) for further sequencing and analysis. The RNA-seq data were processed, assembled, and annotated as described previously (Gao *et al.*, 2016). A total of 261 263 680 clean reads were obtained from six RNA-seq libraries. RNA-seq reads were aligned using a reference genome sequence (*R. chinensis* Jacq. cv Old Blush; https://lipmbrowsers.toulouse.inra.fr/pub/RchiOBHm-V2/). The differentially expressed genes (DEGs; TRV control vs TRV-Rh*LOL1*, fold change > 2, adjusted $P \leq 0.05$) were subjected to further Kyoto Encyclopedia of Genes and Genomes (KEGG) analysis.

Subcellular localization

The coding sequence of Rh*LOL1* was fused with *GFP* and inserted into the pCAMBIA1300 vector harboring a Super promoter (Yue *et al.*, 2012) to construct the *pSuper::*Rh*LOL1-GFP* vector. *NF-YA4-mCherry* was used as a nuclear marker. The vectors were transformed into *Agrobacterium tumefaciens* strain GV3101 and co-infiltrated into *N. benthamiana* leaves. After 3 d of infiltration, the fluorescence signals in the leaf epidermal cells were examined using a laser confocal fluorescence microscope (FluoView FV1000; Olympus, Tokyo, Japan). The primers used to make the constructs are listed in Table S1.

Bimolecular fluorescence complementation assay

Rh*LOL1* was fused with the N-terminus of yellow fluorescence protein (*nYFP*), and Rh*ILR3* was fused with the C-terminus of YFP (*cYFP*), and then inserted into p35S-SPYNE(R)173 vector and p35S-SPYCE(M) vector, respectively. Rh*LOL1-nYFP* and Rh*ILR3-cYFP* were co-transfected into *N. benthamiana* leaves. The YFP fluorescence signals were observed under a microscope (FV3000; Olympus) under 488 nm excitation. The primers used in the biomolecular fluorescence completion (BiFC) are listed in Table S1.

VIGS assay

Gene-specific fragments of Rh*LOL1* (438 bp) and Rh*ILR3* (295 bp) were inserted into the pTRV2 vector to construct pTRV2-Rh*LOL1* and pTRV2-Rh*ILR3*, respectively. The silencing of Rh*LOL1* and Rh*ILR3* was performed in rose plantlets using VIGS, as described previously (Liang *et al.*, 2020). The pTRV2-Rh*LOL1*, pTRV2-Rh*ILR3*, pTRV1, and pTRV2 vectors were transformed into *A. tumefaciens* strain GV3101. The *A. tumefaciens* cells were harvested by centrifugation at 2057 ***g*** for 10 min and then resuspended in infiltration buffer (0.2 mM acetosyringone, 10 mM MES, 10 mM $MgCl_2$, pH 5.6) at a final OD_{600} of 1.0. The pTRV1 and pTRV2 (as control), pTRV1 and pTRV-Rh*LOL1*, and pTRV1 and pTRV2-Rh*ILR3* cultures were mixed in a 1 : 1 (v/v) ratio.

The rose plantlets were transformed by immersing them into the bacterial suspension followed by infiltration under a vacuum at 0.7 MPa. After the infiltration, the plantlets were transplanted into a mixture of vermiculite and nutritive soil (1 : 1). At least 40 plantlets were used for each gene silencing. Before further functional analyses, we measured the expression of target genes by RT-qPCR in the petals at stage 5 in each flower. The flowers with downregulated gene expression levels were used for further analysis.

Tomato transformation and pedicel abscission assay

To generate transgenic tomato plants overexpressing Sl*LOL1* (Es-ind-Sl*LOL1*) using an estradiol-inducible stable transgene system, the coding sequence of Sl*LOL1* was amplified and inserted into the vector pER8. The construct was introduced into *A. tumefaciens* strain GV3101 and transformed into the tomato cultivar 'MicroTom' using an *Agrobacterium*-mediated transformation (Fillatti *et al.*, 1987).

A pedicel abscission assay was performed as described previously (Ma *et al.*, 2015). Tomato inflorescences with at least two newly opened flowers were harvested and placed in a vial containing 10 μM estradiol or DMSO (control) for 12 h. The flowers were removed with a sharp razor blade, and the abscission of the remaining pedicel from the peduncle was monitored.

Yeast two-hybrid assay

A yeast two-hybrid (Y2H) system was used to screen for *Rh*LOL1-interacting proteins in a cDNA library from the rose petal AZ (from a mix of stages 3–6). The coding sequence of Rh*LOL1* was inserted into pGBKT7 (BD) as the bait. The coding sequence of Rh*ILR3* was inserted into pGADT7 (AD) as the prey vector. pGBKT7-T and pGADT7-53 were used as positive controls; pGBKT7 and pGADT7-Rh*ILR3*, and pGBKT7-Rh*LOL1* and pGADT7 were used as negative controls. The bait and prey vectors were co-transformed into the yeast strain Y2H Gold, and the transformants were spotted onto SD/-Trp-Leu, SD/-Trp-Leu-His-Ade, SD/-Trp-Leu-His-Ade + Aureobasidin A (AbA), and SD/-Trp-Leu-His-Ade + AbA + X-gal plates. The primers used in the Y2H assay are listed in Table S1.

Dual-luciferase reporter assay in *N. benthamiana*

For the analysis of the transcription regulatory activity of *Rh*LOL1, the coding sequence (including the stop codon) of Rh*LOL1* was inserted into the pBD vector. The empty vector pBD was used as the negative control.

For the transactivation assay of *Rh*ILR3 and *Rh*LOL1 on the *Aux/IAA* promoters, the promoter sequences were inserted into pGreenII 0800-LUC vectors upstream of the luciferase (*LUC*) gene to construct the Pro*Aux/IAA::LUC* reporter plasmid, including 1761 bp of the Rh*IAA4-1* promoter, 2571 bp of the Rh*IAA4-2* promoter, 2655 bp of the Rh*IAA6* promoter, 1024 bp of the Rh*IAA14* promoter, 1454 bp of the Rh*IAA17* promoter, and 1342 bp of the Rh*Aux28* promoter.

The coding sequences of Rh*ILR3* and Rh*LOL1* were inserted into pGreenII 62-SK vectors to construct the *Pro35S::*Rh*ILR3* and *Pro35S::*Rh*LOL1* effector plasmids, respectively. Empty vector pGreenII 62-SK was used as the negative control. The vectors were transformed into *A. tumefaciens* strain GV3101 harboring both the pSoup and p19 plasmids. The mixed *A. tumefaciens* cultures were co-infiltrated into *N. benthamiana* plants with four to

five young leaves. After 3 d of infiltration, the values of LUC and Renilla luciferase (REN) were analyzed to determine the LUC/REN ratio. The primers used in the dual-LUC analysis are listed in Table S1.

Firefly LUC complementation imaging assay

The coding sequences of Rh*LOL1* and Rh*ILR3* were cloned and constructed into the *Pro35S::nLUC* and *Pro35S::cLUC* vectors to produce fusion proteins (Chen *et al.*, 2008). Rh*ILR3-cLUC* and *nLUC*, *cLUC* and Rh*LOL1-nLUC*, and *nLUC* and *cLUC* were used as negative controls. The negative control combinations and the *Pro35S::nLUC* and *Pro35S::cLUC* pair were co-transformed into *A. tumefaciens* strain GV3101 harboring both the pSoup and p19 plasmids and then infiltrated into the *N. benthamiana* leaves. After 3 d of infiltration, the abaxial surfaces of the *N. benthamiana* leaves were sprayed with 50 mg l^{-1} D-luciferin (Promega) and the luminescence was detected using a CDD camera (ChemiPro HT 1300B/LND, 16 bits; Roper Technologies, Sarasota, FL, USA). The primers used in this assay are listed in Table S1.

Co-immunoprecipitation assay

Agrobacterium tumefaciens cells harboring *Pro35S::*Rh*LOL1-GFP* and *Pro35S::*Rh*ILR3-FLAG* were co-infiltrated into *N. benthamiana* leaves. After 3 d of infiltration, the *N. benthamiana* leaves were harvested, and their total proteins were extracted using protein extraction buffer (5 mM EGTA, 50 mM Tris–HCl (pH 7.5), 10 mM NaF, 10 mM Na_3VO_4, 5% (v/v) glycerinum, 10 mM DTT, 1 mM PMSF, 50 mM β-mercaptoethanol, and 1% (v/v) protease inhibitor cocktail (Roche)). The protein supernatants were incubated with anti-FLAG M2 magnetic beads (M8823; Millipore Sigma, Darmstadt, Germany). Protein extracts were separated on 10% SDS–PAGE gels and then transferred to polyvinylidene difluoride membranes using transferring buffer (39 mM glycine, 48 mM Tris, 0.037% (w/v) SDS, and 20% (v/v) methanol). The membranes were then blocked with skimmed milk for 1 h at room temperature. The target proteins were incubated with anti-GFP (BE2005, 1 : 3000 dilution; Easybio, Beijing, China) or anti-FLAG (BE2070, 1 : 3000 dilution; Easybio) at room temperature for 1 h and sequentially incubated with secondary peroxidase-conjugated anti-mouse antibody (BE0141, 1 : 10 000 dilution; Easybio) at room temperature for 1 h. The primers used in this assay are listed in Table S1.

Chromatin immunoprecipitation-qPCR assay

Chromatin immunoprecipitation (ChIP)-qPCR was performed as described previously (Zhang *et al.*, 2021). An *A. tumefaciens* suspension harboring *pSuper::*Rh*ILR3-GFP* or *pSuper::GFP* was cultured overnight at 28°C and then resuspended in infiltration buffer (10 mM 2-(N-morpholino)-ethanesulfonic acid, 10 mM $MgCl_2$, 0.2 mM acetosyringone, pH 5.6). The suspensions were adjusted to OD_{600} = 1.0 and infiltrated into rose plantlets under a vacuum at 0.7 MPa. After 3 d growth, a 2-g sample of the transformed rose plantlets was cross-linked in 1% (v/v) formaldehyde. The chromatin was interrupted into small fragments in the range of 400–750 bp and then immunoprecipitated with anti-GFP antibody (BE2005, 1 : 100 dilution; Easybio) overnight at 4°C. The chip magnetic beads (Sigma) enriched with targeted DNA were collected, washed, and finally eluted. The eluent was incubated at 65°C for 6 h to reverse the crosslinking. The coprecipitated DNA was purified by PCR Purification Kit (Qiagen) and analyzed using qPCR. The primers used in the ChIP-qPCR assay are listed in Table S1.

Electrophoretic mobility shift assay

The Rh*ILR3* coding sequence was fused with *GST*, inserted into the pGEX-4T-2 vector, and expressed in *Escherichia coli*. The expression of the fused protein was induced using 0.2 mM isopropylthio-β-galactoside, and the cells were cultured overnight at 16°C. The fusion protein was extracted and purified using GST beads Glutathione Sepharose 4B (GE Healthcare, Chicago, IL, USA), according to the manufacturer's instructions. The electrophoretic mobility shift assay (EMSA) was performed using a Chemiluminescent Nucleic Acid Detection Module Kit (Thermo Fisher Scientific), according to the manufacturer's instructions. The biotin-labeled probes were designed as described in Table S1.

Accession numbers

The gene sequences and raw reads of the RNA-seq data were deposited into the GenBank database (https://www.ncbi.nlm.nih.gov/geo/) under the following accession numbers: Rh*LOL1* (OM864511), Rh*ILR3* (OM864512), and raw reads of RNA-seq (PRJNA810333).

Results

Cytokinin is an accelerator of petal abscission in rose

To understand the function of CK in rose petal abscission, we explored the CK contents of an abscission-prone rose cultivar ('Golden Shower') during flowering. The flowering process, from opening to abscission, was categorized into six stages, as described previously (Gao *et al.*, 2016; Liang *et al.*, 2020). We first measured the contents of four biologically active forms of CKs in the petal AZ during flower opening and abscission using LC–MS/MS. Of these CKs, iP, *trans*-zeatin (tZ), and dihydrozeatin (DZ) could be detected in the petal AZ, while *cis*-zeatin could not be detected (Fig. 1a). The levels of iP in the petal AZ were significantly increased in stages 5 and 6 compared with stage 3, while the contents of tZ and DZ did not significantly change during flower abscission (Fig. 1a). The distribution of iP in the petal AZ was also investigated using immunolocalization, which confirmed these findings through the presence of a stronger immunolabeling signal at stage 5 than at stage 3 (Fig. 1b).

We further examined the effects of an exogenous iP treatment on rose petal abscission. We observed that the period between observing fully opened flowers to complete petal abscission was

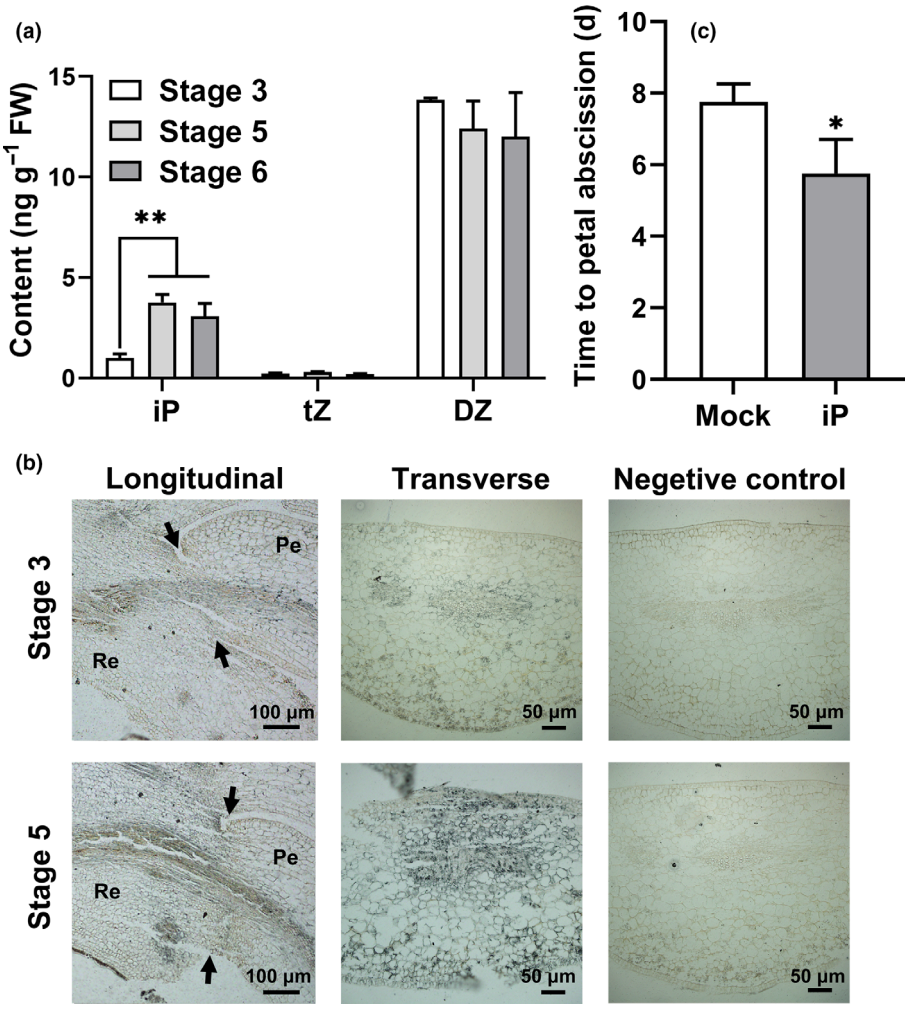

Fig. 1 Cytokinin (CK) accelerates petal abscission in rose. (a) CK levels in petal abscission zones (AZs) at stages 3, 5, and 6 of flower opening. The CK contents were analyzed using liquid chromatography–mass spectrometry (LC–MS)/MS. Statistically significant differences between stage 5/6 and stage 3 were determined using a two-tailed Student's *t*-test (**, $P < 0.01$). DZ, dihydrozeatin; iP, N6-(Δ2-isopentenyl)-adenine; tZ, *trans*-zeatin. (b) Immunolocalization of N6-(Δ^2-isopentenyl)-adenine (iP) in the petal AZ at stage 3 or stage 5 of flower opening, using an anti-iP antibody to detect the immuno-gold localization. Longitudinal images were longitudinal sections of petal bases including petal (Pe), petal AZs, and receptacle (Re). Arrows indicate the petal AZs. Transverse images and negative controls were transverse sections of petal AZs. (c) Effect of iP treatment on rose petal abscission. Flowers at stage 2 were treated with 10 μM iP, or dimethyl sulfoxide as a mock treatment. Statistically significant differences between the iP and mock treatments were determined by two-tailed Student's *t*-test (*, $P < 0.05$). Data in (a, c) are shown as mean ± SD.

shorter under the iP treatment than under the mock treatment (Fig. 1c). The results indicated that CK, especially iP, is an accelerator of petal abscission in rose.

The expression of Rh*LOL1* is induced following petal abscission and exogenous CK treatment

To elucidate the molecular basis by which CKs regulate petal abscission, we explored the expression of the DEGs identified in our previously-reported petal abscission transcriptome (Gao *et al.*, 2016) in response to CK treatment. We identified that the expression of a LSD1 family member, Rh*LOL1*, was significantly induced by 6-BA (Fig. 2a). In addition, we observed that Rh*LOL1* was much more highly expressed in the AZ and receptacle than in the petals themselves (Fig. 2b), and that its expression in the petal AZ was significantly increased during flower opening (Fig. 2c). We also tested the expression of other *LSD* family members, Rh*LSD1* and Rh*LOL2*, in the petal AZ during flower abscission, and observed a different expression pattern to Rh*LOL1*, suggesting no redundant function among Rh*LOL1* and Rh*LSD1* or Rh*LOL2* in petal abscission (Fig. S1).

A phylogenetic analysis indicated that the *Rh*LOL1 protein belongs to the LSD1 family and contains three zinc finger LSD domains (Fig. S2a,b). *Rh*LOL1 shares a high sequence similarity with *At*LOL1 in Arabidopsis (Fig. S2a). We tested the subcellular localization of *Rh*LOL1 by expressing the fusion protein *Rh*LOL1-GFP in *N. benthamiana* leaves, showing that the *Rh*LOL1-GFP signal overlapped with the signal derived from a nucleus marker protein NF-YA4 fused with mCherry (Fig. 2d). In addition, the *Rh*LOL1-GFP signal was also observed in the cytoplasm (Fig. 2d), indicating that *Rh*LOL1 localizes to the nucleus and the cytoplasm.

We further tested the transcriptional activity of *Rh*LOL1 using a dual-LUC transactivation assay with the GAL4-binding domain (BD). We constructed the effector plasmid pBD-Rh*LOL1* and co-infiltrated the reporter construct into *N. benthamiana* leaves (Fig. 2e). We observed significantly higher firefly LUC activity than pBD alone (Fig. 2f), indicating that *Rh*LOL1 is a transcriptional activator.

Silencing Rh*LOL1* delays petal abscission

To explore the function of Rh*LOL1* in petal abscission, we suppressed its endogenous expression in rose using VIGS. The Rh*LOL1*-silencing construct reduced the expression of Rh*LOL1* in the transformed petals compared with those transformed with

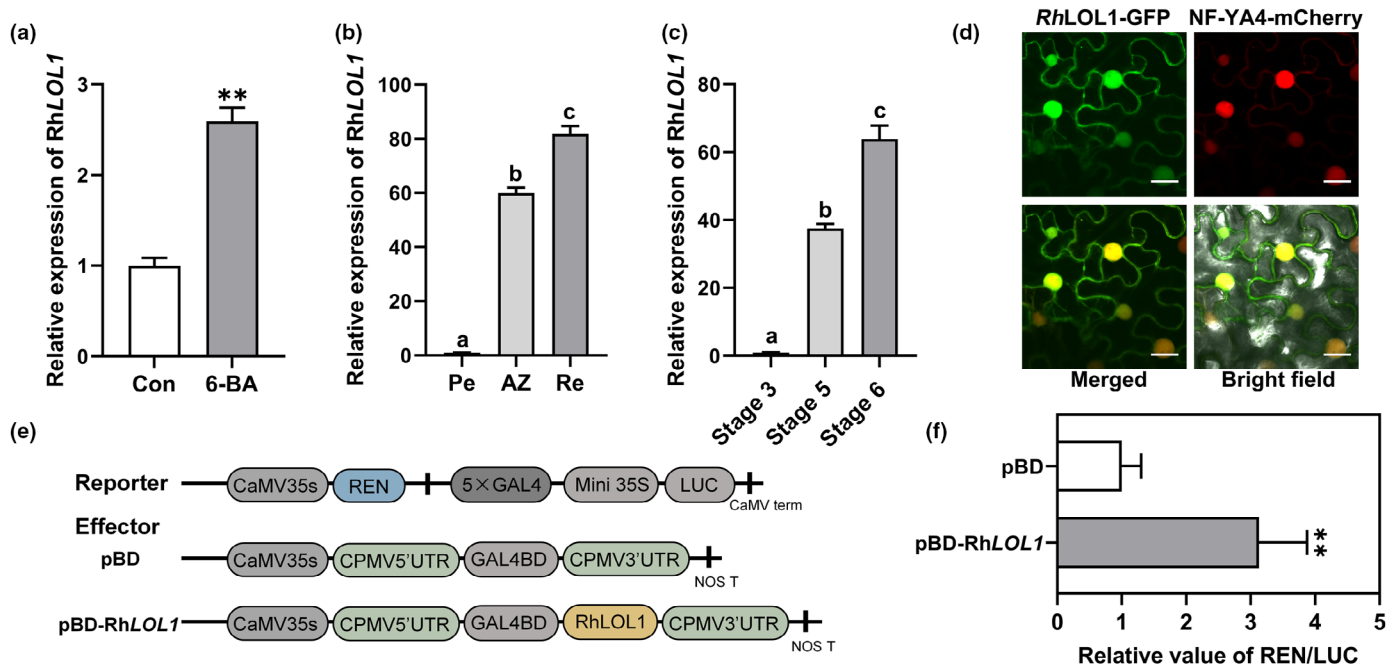

Fig. 2 Expression of Rh*LOL1*, and localization and transactivation of *Rh*LOL1. (a) Reverse transcription polymerase chain reaction (RT-qPCR) analysis of Rh*LOL1* expression in response to 6-benzyl aminopurine (6-BA) treatment. Flowers at stage 2 were treated with 100 μM 6-BA for 24 h. The statistically significant difference was determined by two-tailed Student's *t*-test (**, $P < 0.01$). (b, c) RT-qPCR analysis of Rh*LOL1* expression in different organs at stage 5, and in petal AZs at different stages; Pe, petal; AZ, abscission zone; Re, receptacle. Letters indicate significant differences determined using a Tukey–Kramer test ($P < 0.05$). (d) *Rh*LOL1 is localized in the cytoplasm and nucleus. Rh*LOL1-GFP* and the nuclear marker *NF-YA4-mCherry* were co-expressed in *Nicotiana benthamiana* leaves. Bars, 20 μm. (e) Schematic representation of the reporter and effector constructs for the analysis of the transcriptional regulatory activity of *Rh*LOL1. The reporter vector includes an internal control *Renilla luciferase* driven by CaMV35s promoter, five copies of GAL4-binding element, and a minimal CaMV35s promoter driving *luciferase*. The Rh*LOL1* open reading frame sequence was inserted into pBD vector driven by CaMV35s promoter as the effector (pBD-RhLOL1). (f) Transcriptional activity analysis of *Rh*LOL1 in *N. benthamiana* leaves. Data in (a, b, c, f) are shown as mean ± SD. Asterisks indicate a statistically significant difference, determined by two-sided Student's *t*-test (**, $P < 0.01$).

the TRV empty vector control (Fig. 3a). In the Rh*LOL1*-silenced plants, the time from fully opened flowers to the abscission of all petals was 11.3 ± 2.5 d, compared with 8.2 ± 0.7 d in the TRV control (Fig. 3b,c), indicating that silencing Rh*LOL1* delays petal abscission.

We next investigated whether the Rh*LOL1* ortholog in tomato, Sl*LOL1* (Solyc08g077060.3.1, Fig. S2c), has a conserved function in floral organ abscission. We generated transgenic tomato lines overexpressing Sl*LOL1* under an estradiol-inducible stable transgene system (Es-ind-Sl*LOL1*). Reverse transcription polymerase chain reaction analysis confirmed that the transcript levels of Sl*LOL1* were significantly higher in the Es-ind-Sl*LOL1* lines than in the wild-type plants after 12 h of estradiol treatment (Fig. 3d). We observed that, 11 h after flowers were manually removed, 95.0% and 97.6% of estradiol-treated pedicels had abscised in Es-ind-Sl*LOL1* lines #2 and #5, respectively, whereas only 68% and 74% of the DMSO-treated (control) pedicels in lines #2 and #5, respectively, had abscised in the same period (Fig. 3e).

*Rh*ILR3 interacts with *Rh*LOL1 to influence petal abscission

Previous studies suggested that the zinc finger LSD domains in LSD1 proteins might be responsible for protein binding (Czarnocka *et al.*, 2017). We therefore screened potential *Rh*LOL1 interactors in a petal AZ yeast library using the Y2H system. Among the putatively interacting proteins, we noticed that *Rh*ILR3 was identified seven times independently (Table S2). A phylogenetic analysis showed that *Rh*ILR3 was sequentially similar to IAA-LEUCINE RESISTANT3 (*At*ILR3) from Arabidopsis, a basic helix–loop–helix (bHLH) transcription factor in subfamily IV (Fig. S3). We confirmed the interaction between *Rh*LOL1 and *Rh*ILR3 *in vitro* using Y2H (Fig. 4a). Luciferase complementation imaging (LCI) and co-immunoprecipitation assay were also used to further confirm their interaction *in vivo* (Fig. 4b,c). Moreover, BiFC assay showed that *Rh*LOL1 interacted with *Rh*ILR3 in the nucleus of transgenic *N. benthamiana* leaves (Fig. 4d).

To investigate the function of Rh*ILR3* in petal abscission, we first examined its expression in the different flower opening stages and organs, including petals, petal AZ, and receptacles, using RT-qPCR. We found that the expression of Rh*ILR3* was similar in all the tested stages and organs (Fig. 5a). An investigation of its subcellular localization in transgenic *N. benthamiana* leaves showed that *Rh*ILR3 was localized in the nucleus (Fig. 5b). We then investigated the effect of Rh*ILR3* silencing on petal abscission using VIGS. A RT-qPCR confirmed that, compared with the TRV control, the expression of Rh*ILR3* was reduced in the Rh*ILR3*-silenced petals (Fig. 5c). We observed that the time from the fully opened flowers to the abscission of all petals was decreased in the Rh*ILR3*-

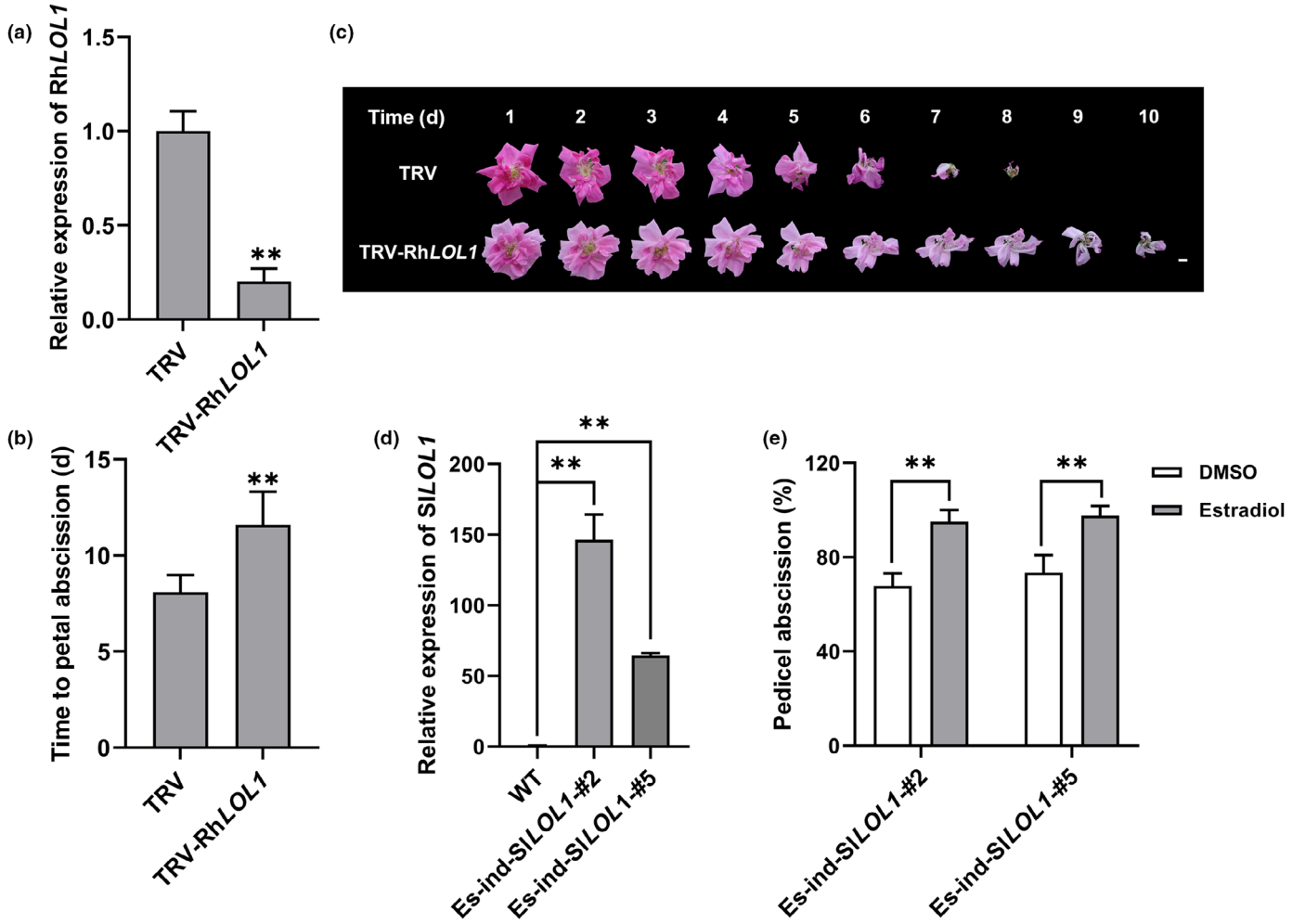

Fig. 3 Effects of the ectopic expression of Rh*LOL1* and Sl*LOL1* on floral organ abscission in rose and tomato. (a) Reverse transcription polymerase chain reaction (RT-qPCR) analysis of the TRV control and Rh*LOL1*-silenced rose (TRV-Rh*LOL1*). Rh*UBI2* was used as the internal control. (b) Time from the appearance of the fully opened flowers to the abscission of all petals in the Rh*LOL1*-silenced rose and TRV control. (c) Flower phenotypes of the TRV control and Rh*LOL1*-silenced rose. The photographs were taken daily. Bar, 1 cm. (d) RT-qPCR analysis of the wild-type (WT) and estradiol-induced Sl*LOL1*-overexpressing tomato (Es-ind-Sl*LOL1*). Sl*SAND* was used as an internal control. (e) Percentage of tomato pedicels abscised at 11 h after flower removal. The pedicels were harvested and treated with 10 μM estradiol or DMSO (control) for 12 h before flower removal. For (a, b, e), the asterisks indicate statistically significant differences between TRV and TRV-Rh*LOL1* (a, b) or the DMSO and estradiol treatments (e), determined using a two-tailed Student's *t*-test (**, $P < 0.01$). For (d), the asterisks indicate statistically significant differences between the WT and Es-ind-Sl*LOL1*-#2 or Es-ind-Sl*LOL1*-#5, determined by Dunnett test (**, $P < 0.01$). Data in (a, b, d, e) are shown as mean ± SD.

silenced plants compared with the TRV control (5.25 ± 0.83 d and 7.25 ± 0.43 d, respectively; Fig. 5d,e).

The *Rh*LOL1–*Rh*ILR3 module directly activates the expression of *Aux/IAA* genes

We conducted an RNA-seq analysis to identify DEGs (fold change ≥ 2, adjusted $P \leq 0.05$) between the TRV and Rh*LOL1*-silenced plants (Table S3). We identified 2144 downregulated and 2820 upregulated genes in the Rh*LOL1*-silenced plants relative to the TRV control plants. A KEGG analysis showed that the term 'plant hormone signal transduction' was significantly enriched in these DEGs and was associated with 85 of them (Fig. S4a). Among these, 41 genes were involved in the auxin signaling pathway, including nine *Aux/IAA* genes (Table S4), suggesting a potential connection between Rh*LOL1* and the auxin signaling pathway, especially the Aux/IAAs. We validated the RNA-seq results using RT-qPCR, confirming that the expression levels of seven *Aux/IAA* genes were reduced in the Rh*LOL1*-silenced plants (Fig. S4b).

We next investigated whether *Rh*LOL1 and *Rh*ILR3 directly target *Aux/IAA*s. The *Rh*LOL1 protein does not have a typical DNA-binding domain; therefore, we attempted to test the binding of *Rh*ILR3 with the promoters of the differentially expressed *Aux/IAA*s identified above. We identified the promoters of these *Aux/IAA*s in the rose genome database (https://lipmbrowsers.toulouse.inra.fr/pub/RchiOBHm-V2/) and searched them for the presence of the G-box element (CACGTG), and more generally the E-box (CANNTG), which have both been reported to be binding sites for bHLH transcription factors (Hao *et al.*, 2021).

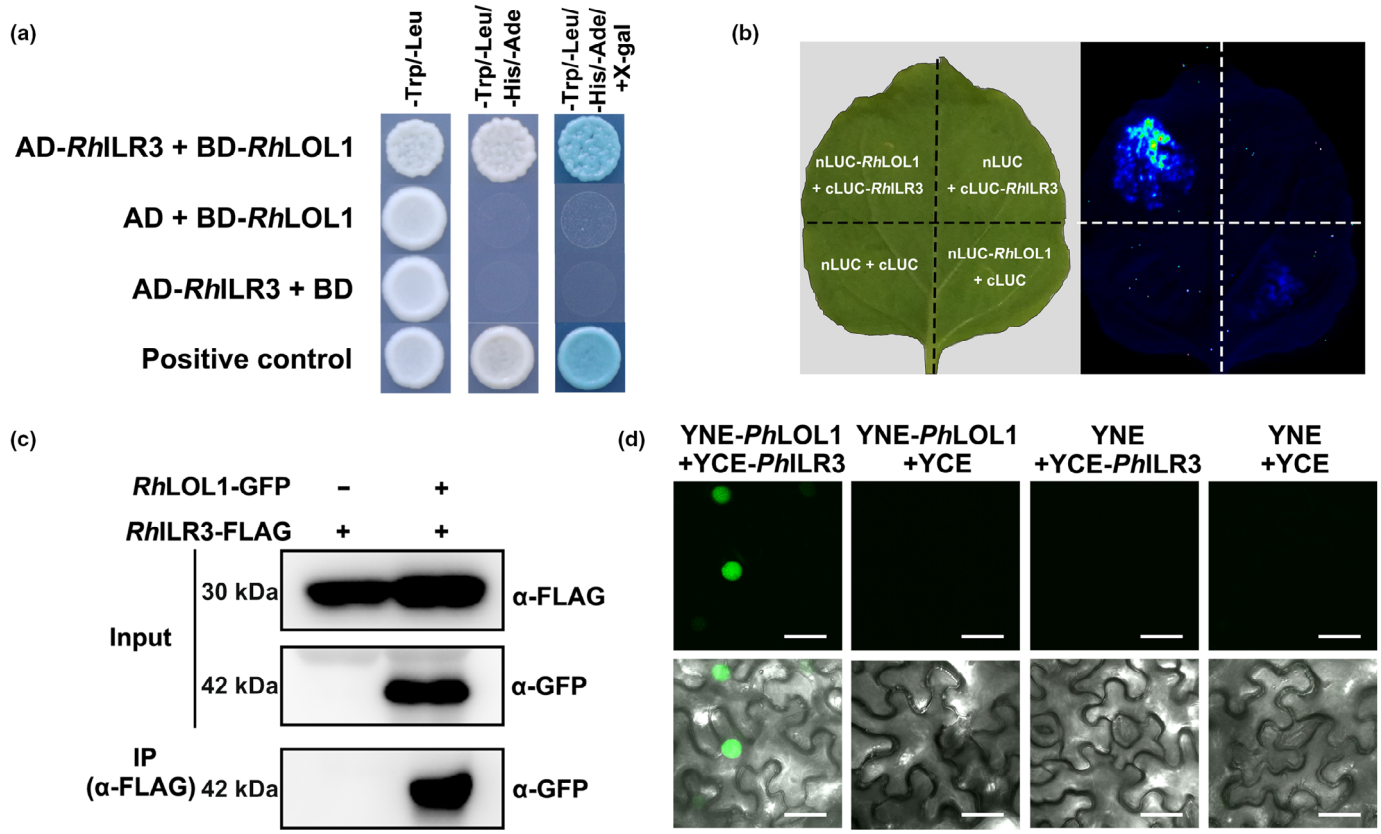

Fig. 4 *Rh*LOL1 interacts with *Rh*ILR3. (a) Interaction of *Rh*LOL1 and *Rh*ILR3 analyzed using a yeast two-hybrid assay. The AD is an empty pGADT7 vector. The binding domain (BD) is an empty pGBKT7 vector. The positive control is pGBKT7-53 + pGADT7-T. (b) Interaction of *Rh*LOL1 and *Rh*ILR3 analyzed using a firefly LUC complementation imaging assay. Rh*ILR3-cLUC* and Rh*LOL1-nLUC* were co-infiltrated into *Nicotiana benthamiana* leaves. *Rh*ILR3-cLUC and nLUC, cLUC and *Rh*LOL-nLUC, or nLUC and cLUC were used as negative controls. (c) Interaction of *Rh*LOL1 and *Rh*ILR3, analyzed using co-immunoprecipitation. The Rh*LOL1-GFP* and Rh*ILR3-FLAG* were co-infiltrated into *N. benthamiana* leaves. The total proteins were extracted after 3 d of infiltration, and the supernatant containing the soluble proteins was incubated with anti-FLAG antibodies. The precipitates were analyzed using western blotting with anti-FLAG and anti-GFP antibodies. (d) Interaction of *Rh*LOL1 and *Rh*ILR3, analyzed using bimolecular fluorescence complementation assay. Rh*LOL1-nYFP* and Rh*ILR3-cYFP* were co-infiltrated in *N. benthamiana* leaves. The leaves were visualized using confocal microscopy after 3 d of infiltration. *Rh*LOL1-nYFP with cYFP and nYFP with *Rh*ILR3-cYFP were used as negative controls. Bars, 20 μm.

The promoters of six *Aux/IAA* genes contained G-box and E-box motifs: Rh*IAA4-1*, Rh*IAA4-2*, Rh*IAA6*, Rh*IAA14*, Rh*IAA17*, and Rh*Aux28* (Fig. S5). The ChIP experiments were conducted to assess the interaction of *Rh*ILR3 with those six *Aux/IAA* promoters. We observed that *Rh*ILR3 bound *in vivo* to the promoters of Rh*IAA4-1*, Rh*IAA4-2*, and Rh*IAA17* with a significantly higher DNA-binding ratio than control (*Pro35S::GFP*), while *Rh*ILR3 did not bind to the promoters of Rh*IAA6*, Rh*IAA14*, or Rh*Aux28* (Fig. 6a). We confirmed the results of the ChIP using EMSAs, which again showed that *Rh*ILR3 binds to the G-box biotin-labeled probes on the promoters of Rh*IAA4-1*, Rh*IAA4-2*, and Rh*IAA17*. The binding of *Rh*ILR3 to the G-box motifs of these three promoters was specific, as *Rh*ILR3 failed to bind to mutant probes for the three promoters (Fig. 6b).

We then analyzed how *Rh*ILR3 regulates the activity of these three *Aux/IAA* promoters using a dual-LUC reporter assay. We observed that, upon co-transformation with *Rh*ILR3, the LUC activities derived from the Rh*IAA4-1* and Rh*IAA17* promoters were significantly reduced, while the LUC activity derived from the Rh*IAA4-2* promoter was not significantly changed, compared with the SK controls (Fig. 7a). The results indicated that *Rh*ILR3 alone may be a repressor of Rh*IAA4-1* and Rh*IAA17* expression. Indeed, we observed that the expression levels of Rh*IAA4-1* and Rh*IAA17* were upregulated in Rh*ILR3*-silenced plants, while the expression of Rh*IAA4-2* in these lines was not significantly different from that of the TRV control (Fig. 7b).

To determine whether *Rh*LOL1 plays a role in the *Rh*ILR3-mediated regulation of *Aux/IAA* promoter activities, we co-infiltrated a firefly LUC reporter driven by the *Aux/IAA* promoters with an effector construct harboring *Rh*ILR3 and *Rh*LOL1 in *N. benthamiana* leaves. We observed that the cells co-transformed with both *Rh*ILR3 and *Rh*LOL1 resulted in significantly higher LUC activities than cells transformed with *Rh*ILR3 alone for all three *Aux/IAA* promoters as effectors (Fig. 7c). Our results demonstrated that the *Rh*LOL1–*Rh*ILR3 module functions as an activator that directly regulates the expression of *Aux/IAA* genes.

Silencing Rh*IAA4-1* delays petal abscission

To elucidate whether the identified *Aux/IAAs* participate in CK-induced petal abscission, we first explored the expression of Rh*IAA4-1*, Rh*IAA4-2*, and Rh*IAA17* in response to CK

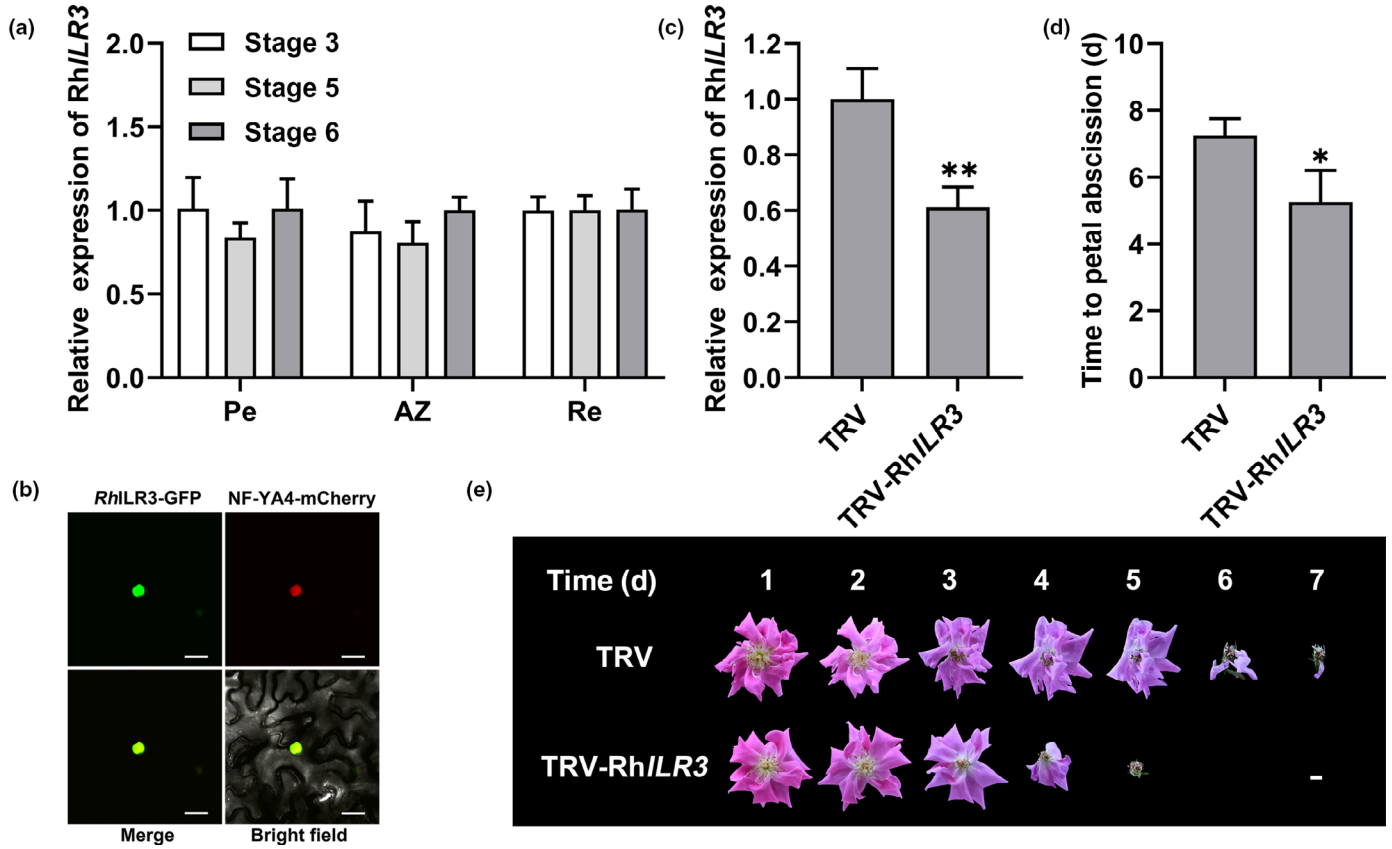

Fig. 5 Silencing Rh*LR3* promotes petal abscission in rose. (a) Reverse transcription polymerase chain reaction (RT-qPCR) analysis of Rh*LR3* expression in the petal (Pe) abscission zone (AZ) during rose flower opening; Re, receptacle. (b) Subcellular localization of *Rh*ILR3. Rh*LR3-GFP* and the nuclear marker *NF-YA4-mCherry* were co-expressed in *Nicotiana benthamiana* leaves. The fluorescence was visualized using confocal microscopy after 3 d of infiltration. Bars, 20 μm. (c) RT-qPCR analysis of Rh*LR3* expression in the TRV control and Rh*LR3*-silenced rose plants. Rh*UBI2* was used as the internal control. Asterisks indicate statistically significant differences between TRV and TRV-Rh*LR3*, determined by two-tailed Student's *t*-test (**, $P < 0.01$). (d) Time from the appearance of the fully opened flowers to the abscission of all petals in the Rh*LR3*-silenced rose and the TRV control. Data in (a, c, d) are shown as mean ± SD. Asterisks indicate statistically significant differences between TRV and TRV-Rh*LR3*, determined by two-tailed Student's *t*-test (*, $P < 0.05$). (e) Flower phenotypes of the TRV control and Rh*LR3*-silenced rose plants. The photographs were taken daily. Bar, 1 cm.

treatment. The results showed that CK treatment significantly induced Rh*IAA4-1* expression, whereas it did not alter the expression of Rh*IAA4-2* and Rh*IAA17* (Fig. 8a), suggesting Rh*IAA4-1* might be involved in CK-induced petal abscission. We therefore investigated the effect of Rh*IAA4-1* silencing on petal abscission using VIGS. A RT-qPCR confirmed that the expression of Rh*IAA4-1* was reduced in the Rh*IAA4-1*-silenced petals compared with the TRV control (Fig. 8b). In the Rh*IAA4-1*-silenced plants, the time from fully opened flowers to the abscission of all petals was 9.0 ± 0.63 d, compared with 7.2 ± 0.75 d in the TRV control (Fig. 8c,d).

Discussion

Cytokinins are known to suppress petal senescence in plants, but their function in petal abscission is ambiguous (Zwack & Rashotte, 2013; Patharkar & Walker, 2019). Previous studies demonstrated that CK inhibits rose petal senescence, and that its content was reduced in senescent petals (Singh *et al.*, 1992; Zwack & Rashotte, 2013; Wu *et al.*, 2017). Here, we observed that the levels of a biologically active CK, iP, were increased in the petal-adjacent AZ during flower senescence/abscission (Fig. 1a,b). Furthermore, exogenous iP applications promoted petal abscission (Fig. 1c), demonstrating the promoting effect of this CK on rose petal abscission. It is interesting that during flower senescence/abscission, the dynamic changes in CK contents are totally different in two adjacent organs, the petals and petal AZ, in which senescence and abscission, respectively, are occurring simultaneously. This suggests that CK may recruit different signaling networks to regulate petal senescence and abscission. In our study, we identified a *LSD1*-like gene, Rh*LOL1*, in rose, which was highly expressed in the petal AZ, and could be induced by CK (Fig. 2a,b). The tissue-specific expression pattern of Rh*LOL1* in the AZ and its functional analysis indicated that *Rh*LOL1 is a member of the network involved in CK-induced petal abscission (Fig. 3).

Although the biological functions of *LSD1*-like genes have been widely studied, the molecular mechanisms underlying the activities of their corresponding proteins are still largely unknown. Our study indicated that *Rh*LOL1 may be a transcriptional activator (Fig. 2f), which is consistent with previous suggestions that other LSD1-like proteins may function as either

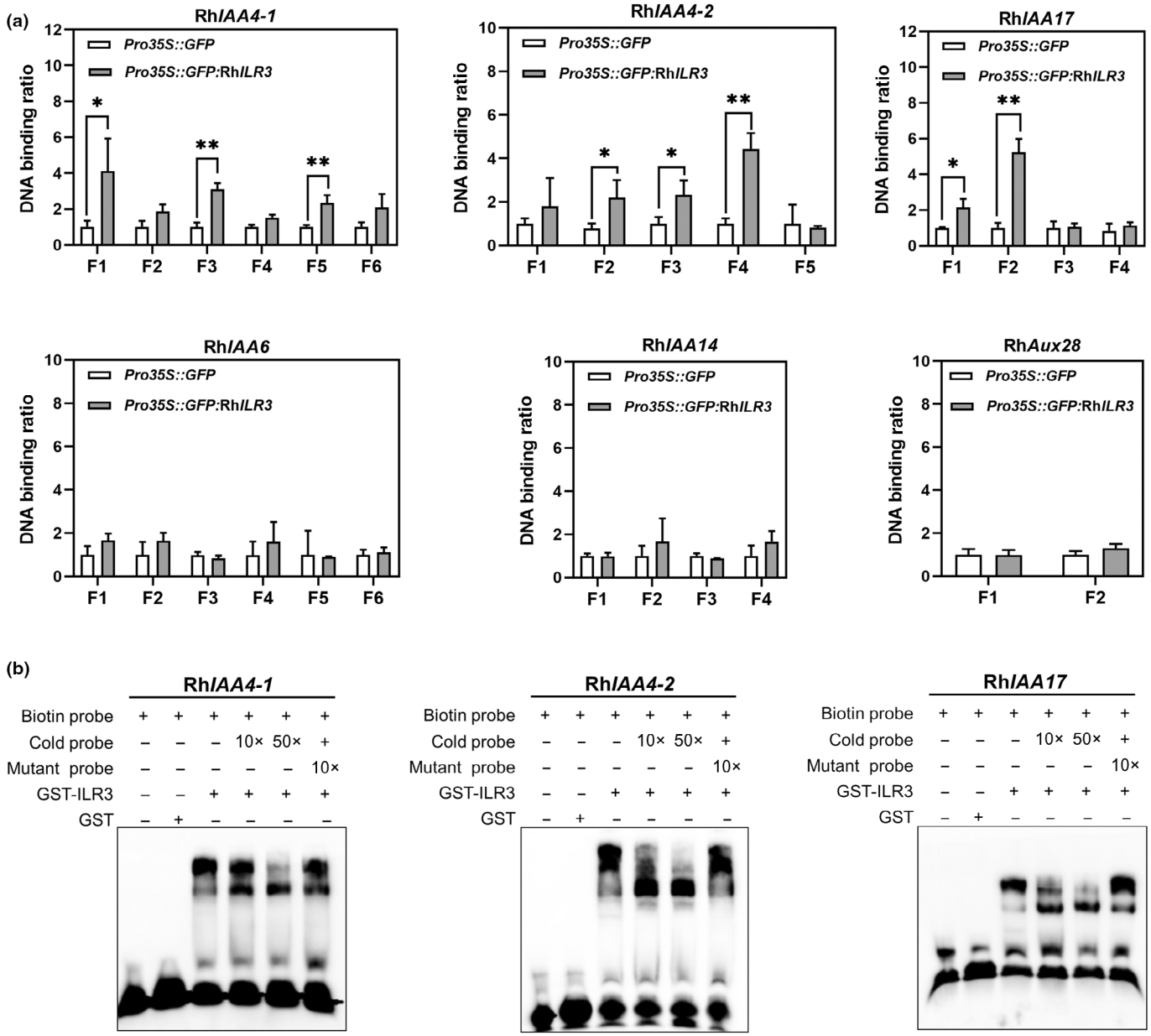

Fig. 6 *Rh*ILR3 binds to the promoters of the *Aux/IAA* genes. (a) ChIP-qPCR analyses of the binding of *Rh*ILR3 to the promoters of the *Aux/IAA* genes. Chromatin was extracted from 2-wk-old rose plantlets expressing *Pro35S::GFP:*Rh*ILR3* using anti-GFP antibodies. The plantlets expressing *Pro35S::GFP* were used as a negative control. Reverse transcription polymerase chain reaction was used to analyze the enrichment of *Rh*ILR3 to the promoters of the auxin/indole-3-acetic acid (*Aux/IAA*) genes. Data are shown as mean ± SD. Asterisks represent statistically significant differences, determined by Student's *t*-test (*, $P < 0.05$; **, $P < 0.01$). (b) Electrophoretic mobility shift assay analyses of *Rh*ILR3 binding to the E-box of the *Aux/IAA* promoters. The competition for binding was performed using unlabeled probes. GST was used as the negative control.

transcriptional regulators or scaffold proteins (Epple *et al.*, 2003). Other studies have indicated that the zinc finger LSD domain is required for the protein–protein interactions and nuclear localization of the LSD1-like proteins (Coll *et al.*, 2010; He *et al.*, 2011; Cabreira *et al.*, 2015). In Arabidopsis, LSD1 interacts with catalases to regulate hypersensitive cell death (Li *et al.*, 2013), while bZIP10 can be excluded from the nucleus by a LSD1–bZIP10 interaction that modulates basal defense and cell death (Kaminaka *et al.*, 2006). We assumed that *Rh*LOL1 works as a transcriptional activator that may not directly bind to the promoters of its targets, as there is no typical DNA-binding domain in *Rh*LOL1; therefore, we identified *Rh*LOL1-interacting proteins and found that a bHLH transcription factor, *Rh*ILR3, can physically interact with *Rh*LOL1. In Arabidopsis, previous studies indicated that ILR3 interacts with other regulators to participate in different metabolic pathways, including iron homeostasis and stress responses (Long *et al.*, 2010; Tissot *et al.*, 2019). The IAA-conjugate-resistant *ilr3-1* (gain-of-function) mutant exhibited reduced sensitivity to IAA-Phe and IAA-Leu. A further analysis indicated that ILR3

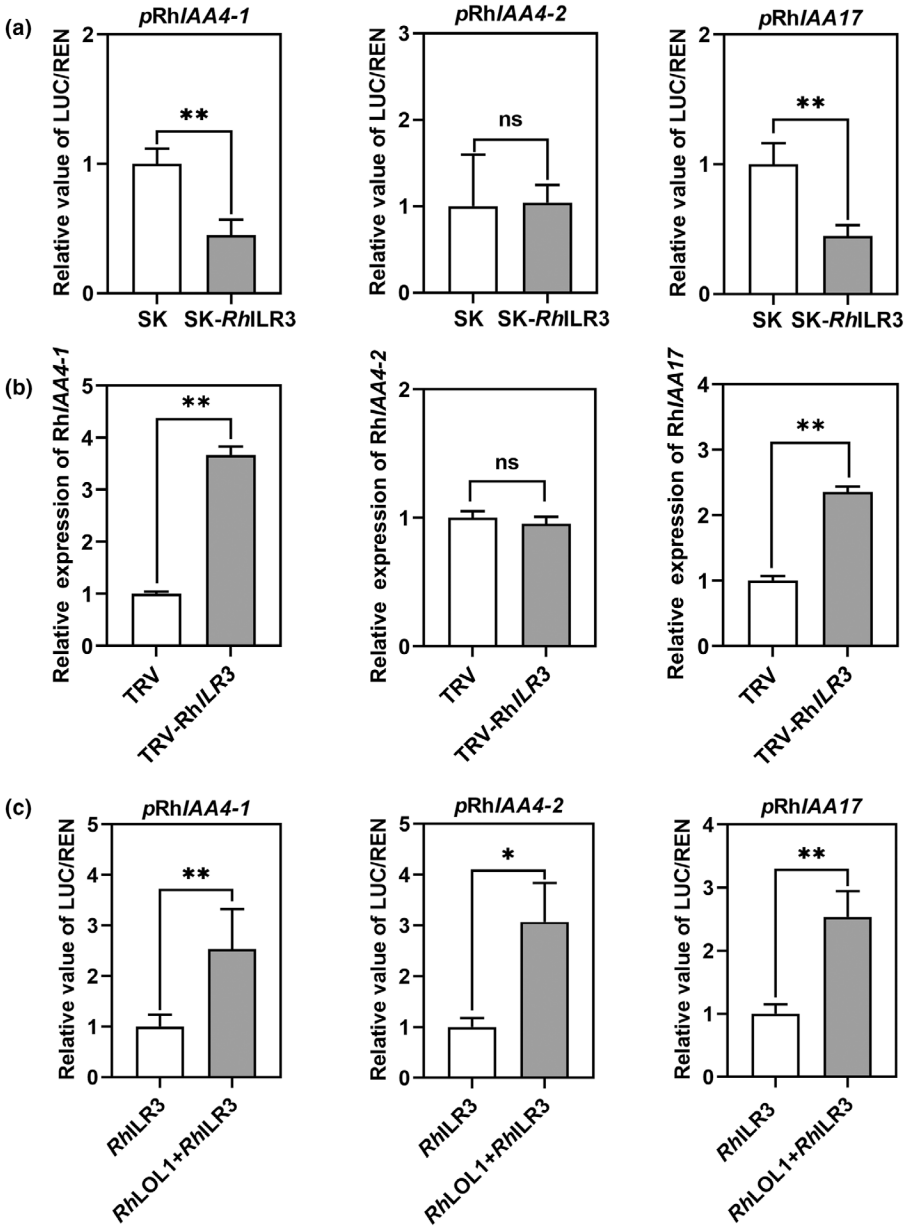

Fig. 7 *Rh*LOL1 and *Rh*ILR3 directly regulate the expression of the *Aux/IAA* genes. (a) Dual-luciferase analysis of the interaction of the *Rh*ILR3 protein with the promoters of the *Aux/IAA* genes. The *ProAux/IAA::LUC* construct was co-infiltrated with *Pro35S::* Rh*ILR3* or the empty SK vector into *Nicotiana benthamiana* leaves. Asterisks indicate statistically significant differences, determined by two-tailed Student's *t*-test (**, $P < 0.01$). (b) The expression of the genes in the TRV control and the Rh*ILR3*-silenced (TRV-Rh*ILR3*) rose plants. Rh*UBI2* was used as the internal control. Asterisks indicate statistically significant differences between TRV and TRV-Rh*ILR3*, determined by two-tailed Student's *t*-test (**, $P < 0.01$; ns, not significant $P > 0.05$). (c) Dual-LUC analyses of the influence of *Rh*LOL1 on the interaction of the *Rh*ILR3 protein and the promoters of the *Aux/IAA* genes. The *ProAux/IAA::LUC* construct and *Pro35S::* Rh*ILR3* were co-infiltrated with *Pro35S::* Rh*LOL1* or the empty SK vector into *N. benthamiana* leaves. Data are shown as mean ± SD. ns, not significant ($P > 0.05$). Asterisks indicate statistically significant differences determined by two-tailed Student's *t*-test (*, $P < 0.05$; **, $P < 0.01$).

regulates the expression of metal transporter genes, thereby indirectly influencing IAA-conjugate hydrolysis (Rampey *et al.*, 2006); however, whether ILR3 directly modulates the auxin pathway was previously unknown. Our results showed *Rh*ILR3 can bind to promoters of Aux/IAA genes as a transcriptional repressor (Figs 6, 7). In addition, we observed that *Rh*ILR3 interacts with *Rh*LOL1 (Fig. 4); however, the promotion of petal abscission by the silencing of Rh*ILR3* (Fig. 5) contrasts with the effect of Rh*LOL1* silencing, which inhibits petal abscission (Fig. 3). This could be explained by the hypothesis that *Rh*ILR3 alone represses the expression of *Aux/IAA*s, while the *Rh*LOL1–*Rh*ILR3 module accelerates their expression.

Previous studies demonstrated that variations in molecular structure and transcription regulation of *Aux/IAA* members contribute to a high complexity of auxin signaling, which further facilitate the diverse functions of Aux/IAAs in response to environment change (Weijers & Wagner, 2016; Luo *et al.*, 2018; Lv *et al.*, 2020). In rose, silencing Rh*IAA16* was reported to effectively promote petal abscission (Gao *et al.*, 2016). But Rh*IAA16* was not included in the DEGs between the TRV and Rh*LOL1*-silenced plants (Table S3). Instead, we identified three *Aux/IAAs* – Rh*IAA4-1*, Rh*IAA4-2*, and Rh*IAA17* – that were directly regulated by the *Rh*LOL1–*Rh*ILR3 module (Fig. 7). Intriguingly, among the three *Aux/IAAs*, only Rh*IAA4-1* expression can be induced by CK treatment (Fig. 8). We speculate that CK-induced *Rh*LOL1 accumulation may be mainly enriched at the promoter of Rh*IAA4-1*, or unknown regulatory modules may participate in the regulation of Rh*IAA4-2* and Rh*IAA17* under the influence of CK. These results imply that Aux/IAA family members are involved in the process of petal abscission in various ways.

In conclusion, we establish that, during the early stages of flower opening, *Rh*ILR3 represses the expression of the *Aux/IAA*s.

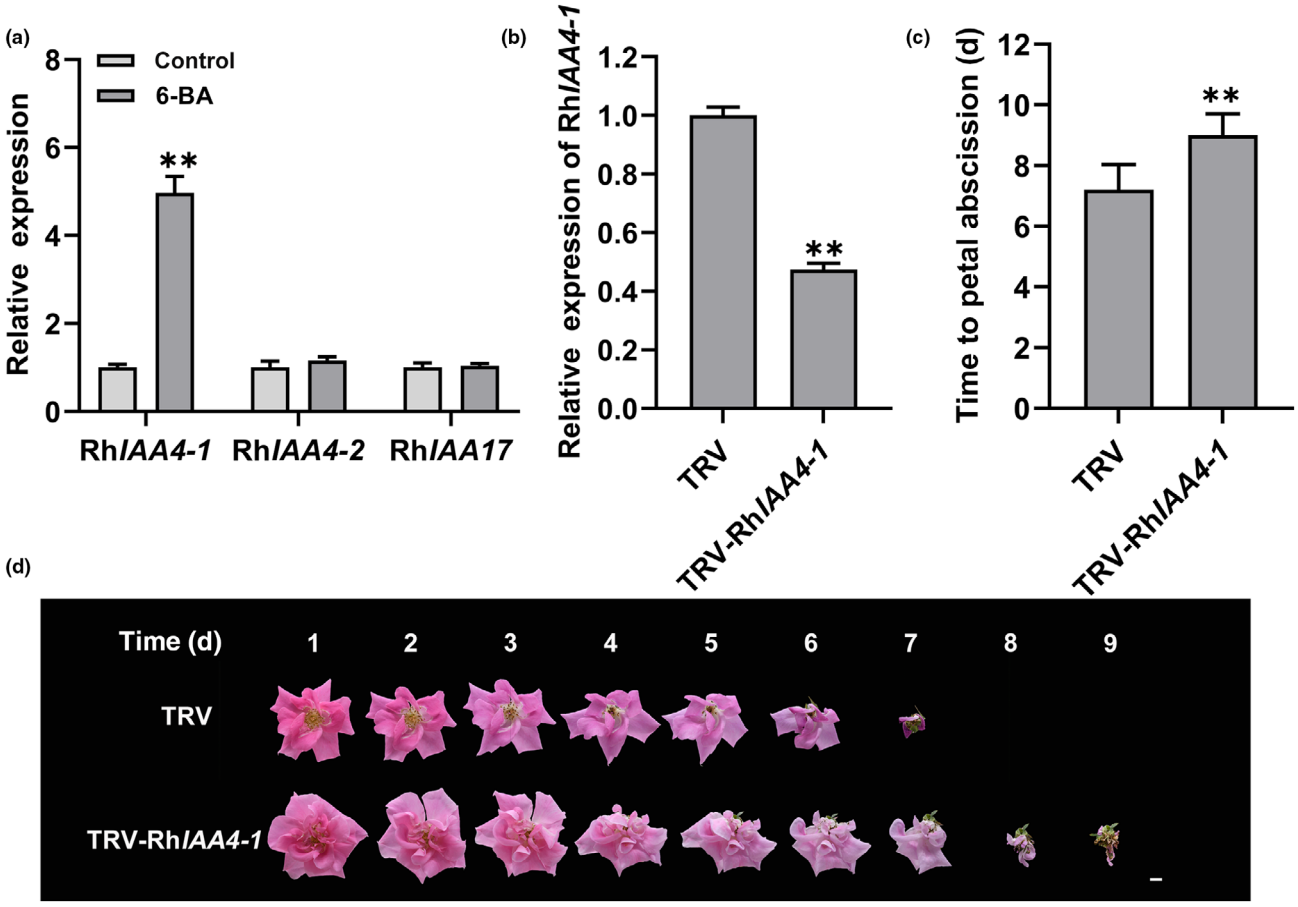

Fig. 8 Silencing Rh*IAA4-1* delays petal abscission in rose. (a) Reverse transcription polymerase chain reaction (RT-qPCR) analysis of expression of Rh*IAA4-1*, Rh*IAA4-2*, and Rh*IAA17* in response to 6-benzyl aminopurine (6-BA) treatment. Flowers at stage 2 were treated with 100 μM 6-BA for 24 h. The statistically significant difference was determined by two-tailed Student's *t*-test (**, $P < 0.01$). (b) RT-qPCR analysis of Rh*IAA4-1* expression in the TRV control and Rh*IAA4-1*-silenced rose plants. Rh*UBI2* was used as the internal control. Asterisks indicate statistically significant differences between TRV and TRV-Rh*IAA4-1*, determined by two-tailed Student's *t*-test (**, $P < 0.01$). (c) Time from the appearance of the fully opened flowers to the abscission of all petals in the Rh*IAA4-1*-silenced rose and the TRV control. Data in (a–c) are shown as mean ± SD. Asterisks indicate statistically significant differences between TRV and TRV-Rh*IAA4-1*, determined by two-tailed Student's *t*-test (*, $P < 0.05$). (d) Flower phenotypes of the TRV control and Rh*IAA4-1*-silenced rose plants. The photographs were taken daily. Bar, 1 cm.

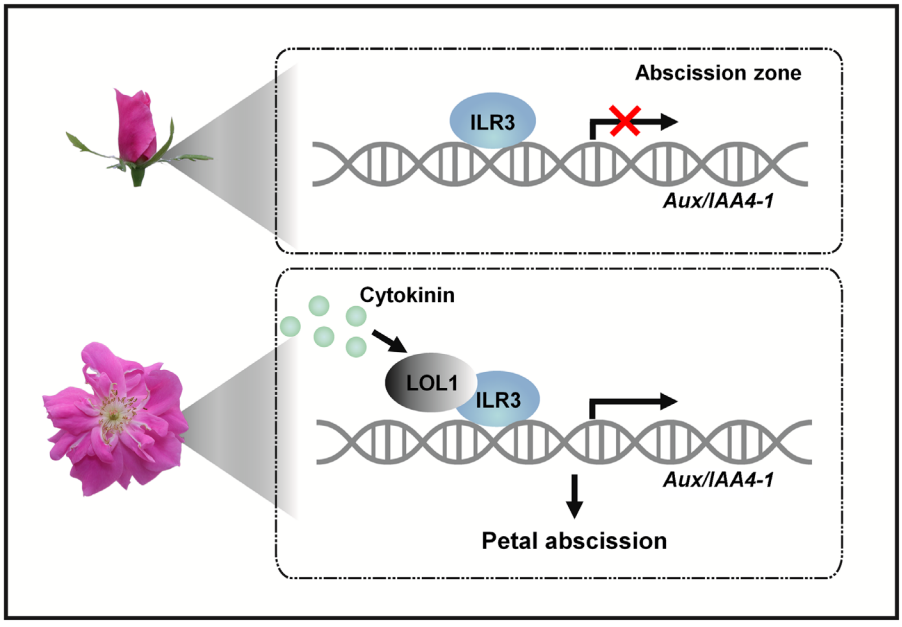

Fig. 9 Model of the *Rh*LOL1–*Rh*ILR3 module regulating cytokinin (CK)-induced petal abscission. During the early stages of flower opening, ILR3 represses the expression of *Aux/IAA4-1*. During flower opening, the expression of *LOL1* is induced by increasing CK levels. LOL1 interacts with ILR3 to activate the expression of *Aux/IAA4-1*, which accelerates CK-induced petal abscission.

During flower opening, the expression of Rh*LOL1* is induced by increasing CK levels. *Rh*LOL1 interacts with *Rh*ILR3 to activate the expression of *Aux/IAA*s, especially Rh*IAA4-1*, which accelerates CK-induced petal abscission (Fig. 9).

Acknowledgements

This work was supported by the National Key Research and Development Program of China (2018YFD1000400), the National Natural Science Foundation of China (31822045 and 31672186), a Key R&D Project grant from Hainan Province (ZDYF2021XDNY169), and the Beijing Municipal Education Commission Construction of Beijing Science and Technology Innovation and Service Capacity in Top Subjects (CEFF-PXM2019_014207_000032).

Competing interests

None declared.

Author contributions

CM and CJ conceived and designed the experiments. CJ performed most of the experiments. Y Liang contributed to the CK measurement and gene functional analyses. SD and SL contributed to the immunolocalization and VIGS assays. Y Liu and HZ contributed to identifying the gene involved in CK-induced petal abscission. JG and C-ZJ provided technical support and conceptual advice. CM and CJ analyzed the data and wrote the article.

ORCID

Junping Gao https://orcid.org/0000-0002-9285-2539
Cai-Zhong Jiang https://orcid.org/0000-0002-5972-7963
Chuyan Jiang https://orcid.org/0000-0003-3381-3262
Yue Liang https://orcid.org/0000-0002-8901-2707
Yang Liu https://orcid.org/0000-0002-6436-1732
Chao Ma https://orcid.org/0000-0002-3866-0894
Haohao Zhao https://orcid.org/0000-0002-2969-9404

Data availability

The data that support the findings of this study are available from the corresponding author upon reasonable request.

References

Bernacki MJ, Rusaczonek A, Czarnocka W, Karpinski S. 2021. Salicylic acid accumulation controlled by LSD1 is essential in triggering cell death in response to abiotic stress. *Cell* **10**: 962.

Borovsky Y, Monsonego N, Mohan V, Shabtai S, Kamara I, Faigenboim A, Hill T, Chen S, Stoffel K, van Deynze A *et al.* 2019. The zinc-finger transcription factor *CcLOL1* controls chloroplast development and immature pepper fruit color in *Capsicum chinense* and its function is conserved in tomato. *The Plant Journal* **99**: 41–55.

Cabreira C, Cagliari A, Bucker-Neto L, Margis-Pinheiro M, de Freitas LB, Bodanese-Zanettini MH. 2015. The phylogeny and evolutionary history of the Lesion Simulating Disease (LSD) gene family in Viridiplantae. *Molecular Genetics Genomics* **290**: 2107–2119.

Chang H, Jones ML, Banowetz GM, Clark DG. 2003. Overproduction of cytokinins in petunia flowers transformed with P(SAG12)-IPT delays corolla senescence and decreases sensitivity to ethylene. *Plant Physiology* **132**: 2174–2183.

Chen H, Zou Y, Shang Y, Lin H, Wang Y, Cai R, Tang X, Zhou JM. 2008. Firefly luciferase complementation imaging assay for protein-protein interactions in plants. *Plant Physiology* **146**: 368–376.

Coll NS, Vercammen D, Smidler A, Clover C, Van Breusegem F, Dangl JL, Epple P. 2010. *Arabidopsis* type I metacaspases control cell death. *Science* **330**: 1393–1397.

Czarnocka W, Van Der Kelen K, Willems P, Szechynska-Hebda M, Shahnejat-Bushehri S, Balazadeh S, Rusaczonek A, Mueller-Roeber B, Van Breusegem F, Karpinski S. 2017. The dual role of LESION SIMULATING DISEASE 1 as a condition-dependent scaffold protein and transcription regulator. *Plant, Cell & Environment* **40**: 2644–2662.

Dal Cin V, Boschetti A, Dorigoni A, Ramina A. 2007. Benzylaminopurine application on two different apple cultivars (*Malus domestica*) displays new and unexpected fruitlet abscission features. *Annals of Botany* **99**: 1195–1202.

Dewitte W, Chiappetta A, Azmi A, Witters E, Strnad M, Rembur J, Noin M, Chriqui D, Van Onckelen H. 1999. Dynamics of cytokinins in apical shoot meristems of a day-neutral tobacco during floral transition and flower formation. *Plant Physiology* **119**: 111–122.

Dietrich RA, Richberg MH, Schmidt R, Dean C, Dangl JL. 1997. A novel zinc finger protein is encoded by the Arabidopsis *LSD1* gene and functions as a negative regulator of plant cell death. *Cell* **88**: 685–694.

van Doorn W. 2001. Categories of petal senescence and abscission: a re-evaluation. *Annals of Botany* **87**: 447–456.

Eisinger W. 1977. Role of cytokinins in carnation flower senescence. *Plant Physiology* **59**: 707–709.

Ellis CM, Nagpal P, Young JC, Hagen G, Guilfoyle TJ, Reed JW. 2005. *AUXIN RESPONSE FACTOR1* and *AUXIN RESPONSE FACTOR2* regulate senescence and floral organ abscission in *Arabidopsis thaliana*. *Development* **132**: 4563–4574.

Epple P, Mack AA, Morris VR, Dangl JL. 2003. Antagonistic control of oxidative stress-induced cell death in *Arabidopsis* by two related, plant-specific zinc finger proteins. *Proceedings of the National Academy of Sciences, USA* **100**: 6831–6836.

Estornell LH, Agusti J, Merelo P, Talon M, Tadeo FR. 2013. Elucidating mechanisms underlying organ abscission. *Plant Science* **199-200**: 48–60.

Fillatti JJ, Kiser J, Rose R, Comai L. 1987. Efficient transfer of a glyphosate tolerance gene into tomato using a binary *Agrobacterium tumefaciens* vector. *Nature Biotechnology* **5**: 726–730.

Gao Y, Liu C, Li X, Xu H, Liang Y, Ma N, Fei Z, Gao J, Jiang CZ, Ma C. 2016. Transcriptome profiling of petal abscission zone and functional analysis of an Aux/IAA family gene *RhIAA16* involved in petal shedding in rose. *Frontiers in Plant Science* **7**: 1375.

Gao Y, Liu Y, Liang Y, Lu J, Jiang C, Fei Z, Jiang CZ, Ma C, Gao J. 2019. *Rosa hybrida* RhERF1 and RhERF4 mediate ethylene- and auxin-regulated petal abscission by influencing pectin degradation. *The Plant Journal* **99**: 1159–1171.

Hao YQ, Zong XM, Ren P, Qian YQ, Fu AG. 2021. Basic helix-loop-helix (bHLH) transcription factors regulate a wide range of functions in Arabidopsis. *International Journal of Molecular Sciences* **22**: 7152.

He S, Huang K, Zhang X, Yu X, Huang P, An C. 2011. The LSD1-type zinc finger motifs of *Pisum sativa* LSD1 are a novel nuclear localization signal and interact with importin alpha. *PLoS ONE* **6**: e22131.

Honig M, Plihalova L, Husickova A, Nisler J, Dolezal K. 2018. Role of cytokinins in senescence, antioxidant defence and photosynthesis. *International Journal of Molecular Sciences* **19**: 4045.

Kaminaka H, Nake C, Epple P, Dittgen J, Schutze K, Chaban C, Holt BF III, Merkle T, Schafer E, Harter K *et al.* 2006. bZIP10-LSD1 antagonism modulates basal defense and cell death in *Arabidopsis* following infection. *EMBO Journal* **25**: 4400–4411.

Lavy M, Estelle M. 2016. Mechanisms of auxin signaling. *Development* **143**: 3226–3229.

Leyser O. 2018. Auxin signaling. *Plant Physiology* **176**: 465–479.

Li Y, Chen L, Mu J, Zuo J. 2013. LESION SIMULATING DISEASE1 interacts with catalases to regulate hypersensitive cell death in Arabidopsis. *Plant Physiology* **163**: 1059–1070.

Liang Y, Jiang C, Liu Y, Gao Y, Lu J, Aiwaili P, Fei Z, Jiang CZ, Hong B, Ma C *et al.* 2020. Auxin regulates sucrose transport to repress petal abscission in rose (*Rosa hybrida*). *Plant Cell* **32**: 3485–3499.

Lim P. 2003. Molecular genetics of leaf senescence in Arabidopsis. *Trends in Plant Science* **8**: 272–278.

Long TA, Tsukagoshi H, Busch W, Lahner B, Salt DE, Benfey PN. 2010. The bHLH transcription factor POPEYE regulates response to iron deficiency in Arabidopsis roots. *Plant Cell* **22**: 2219–2236.

Luo J, Zhou JJ, Zhang JZ. 2018. Aux/IAA gene family in plants: molecular structure, regulation, and function. *International Journal of Molecular Sciences* **19**: 259.

Lv BS, Yu QQ, Liu JJ, Wen XJ, Yan ZW, Hu KQ, Li HB, Kong XP, Li CL, Tian HY *et al.* 2020. Non-canonical AUX/IAA protein IAA33 competes with canonical AUX/IAA repressor IAA5 to negatively regulate auxin signaling. *EMBO Journal* **39**: e101515.

Ma C, Jiang CZ, Gao J. 2021. Regulatory mechanisms underlying activation of organ abscission. *Annual Plant Reviews Online* **4**: 27–56.

Ma C, Meir S, Xiao LT, Tong JH, Liu Q, Reid MS, Jiang CZ. 2015. A KNOTTED1-LIKE HOMEOBOX protein regulates abscission in tomato by modulating the auxin pathway. *Plant Physiology* **167**: 844–853.

Mayak S, Halevy AH. 1970. Cytokinin activity in rose petals and its relation to senescence. *Plant Physiology* **46**: 497–499.

Mor Y, Spiegelstein H, Halevy AH. 1983. Inhibition of ethylene biosynthesis in carnation petals by cytokinin. *Plant Physiology* **71**: 541–546.

Muhlenbock P, Plaszczyca M, Plaszczyca M, Mellerowicz E, Karpinski S. 2007. Lysigenous aerenchyma formation in Arabidopsis is controlled by LESION SIMULATING DISEASE1. *Plant Cell* **19**: 3819–3830.

Muhlenbock P, Szechynska-Hebda M, Plaszczyca M, Baudo M, Mateo A, Mullineaux PM, Parker JE, Karpinska B, Karpinski S. 2008. Chloroplast signaling and LESION SIMULATING DISEASE1 regulate crosstalk between light acclimation and immunity in Arabidopsis. *Plant Cell* **20**: 2339–2356.

Okushima Y, Mitina I, Quach HL, Theologis A. 2005. AUXIN RESPONSE FACTOR 2 (ARF2): a pleiotropic developmental regulator. *The Plant Journal* **43**: 29–46.

Patharkar OR, Walker JC. 2017. Advances in abscission signaling. *Journal of Experimental Botany* **4**: 733–740.

Patharkar OR, Walker JC. 2019. Connections between abscission, dehiscence, pathogen defense, drought tolerance, and senescence. *Plant Science* **284**: 25–29.

Patterson SE, Bleecker AB. 2004. Ethylene-dependent and -independent processes associated with floral organ abscission in Arabidopsis. *Plant Physiology* **134**: 194–203.

Rampey RA, Woodward AW, Hobbs BN, Tierney MP, Lahner B, Salt D, Bartel B. 2006. An Arabidopsis basic helix-loop-helix leucine zipper protein modulates metal homeostasis and auxin conjugate responsiveness. *Genetics* **174**: 1841–1857.

Singh S, Letham DS, Palni LMS. 1992. Cytokinin biochemistry in relation to leaf senescence. VII. Endogenous cytokinin levels and exogenous applications of cytokinins in relation to sequential leaf senescence of tobacco. *Journal of Plant Physiology* **86**: 388–397.

Taverner E, Letham DS, Wang J, Cornish E, Willcocks DA. 1999. Influence of ethylene on cytokinin metabolism in relation to *Petunia* corolla senescence. *Phytochemistry* **51**: 341–347.

Tissot N, Robe K, Gao F, Grant-Grant S, Boucherez J, Bellegarde F, Maghiaoui A, Marcelin R, Izquierdo E, Benhamed M *et al.* 2019. Transcriptional integration of the responses to iron availability in Arabidopsis by the bHLH factor ILR3. *New Phytologist* **223**: 1433–1446.

Torres MA, Jones JD, Dangl JL. 2005. Pathogen-induced, NADPH oxidase-derived reactive oxygen intermediates suppress spread of cell death in *Arabidopsis thaliana*. *Nature Genetics* **37**: 1130–1134.

Wang L, Pei Z, Tian Y, He C. 2005. OsLSD1, a rice zinc finger protein, regulates programmed cell death and callus differentiation. *Molecular Plant–Microbe Interactions* **18**: 375–384.

Weijers D, Wagner D. 2016. Transcriptional responses to the auxin hormone. *Annual Review of Plant Biology* **67**: 539–574.

Wituszyńska W, Ślesak I, Vanderauwera S, Szechyńska-Hebda M, Kornaś A, Van Der Kelen K, Mühlenbock P, Karpińska B, Maćkowski S, Van Breusegem F *et al.* 2013. Lesion simulating disease1, enhanced disease susceptibility1, and phytoalexin deficient4 conditionally regulate cellular signaling homeostasis, photosynthesis, water use efficiency, and seed yield in Arabidopsis. *Plant Physiology* **161**: 1795–1805.

Woltering EJ, van Doorn WG. 1988. Role of ethylene in senescence of petals—morphological and taxonomical relationships. *Journal of Experimental Botany* **39**: 1605–1616.

Wu L, Ma N, Jia Y, Zhang Y, Feng M, Jiang CZ, Ma C, Gao J. 2017. An ethylene-induced regulatory module delays flower senescence by regulating cytokinin content. *Plant Physiology* **173**: 853–862.

Xu J, Chen L, Sun H, Wusiman N, Sun W, Li B, Gao Y, Kong J, Zhang D, Zhang X *et al.* 2019. Crosstalk between cytokinin and ethylene signaling pathways regulates leaf abscission in cotton in response to chemical defoliants. *Journal of Experimental Botany* **70**: 1525–1538.

Yue Y, Zhang M, Zhang J, Tian X, Duan L, Li Z. 2012. Overexpression of the AtLOS5 gene increased abscisic acid level and drought tolerance in transgenic cotton. *Journal of Experimental Botany* **63**: 3741–3748.

Zhang Y, Wu Z, Feng M, Chen J, Qin M, Wang W, Bao Y, Xu Q, Ye Y, Ma C *et al.* 2021. The circadian-controlled PIF8-BBX28 module regulates petal senescence in rose flowers by governing mitochondrial ROS homeostasis at night. *Plant Cell* **33**: 2716–2735.

Zwack PJ, Rashotte AM. 2013. Cytokinin inhibition of leaf senescence. *Plant Signaling & Behavior* **8**: e24737.

Supporting Information

Additional Supporting Information may be found online in the Supporting Information section at the end of the article.

Fig. S1 Expression patterns of *LSD1* family genes in the petal abscission zones at different stages of rose flower opening.

Fig. S2 Phylogenetic tree and alignment analysis of the deduced amino acid sequences of *Rh*LOL1 and its orthologs.

Fig. S3 Phylogenetic tree and motif analysis of *Rh*ILR3.

Fig. S4 Silencing Rh*LOL1* significantly affects the auxin signaling pathway in rose.

Fig. S5 Promoter structure diagrams of the *AUX/IAA* genes in rose.

Table S1 List of primers used in this study.

Table S2 Yeast two-hybrid screening of *Rh*LOL1-interacting proteins in rose.

Table S3 Differentially expressed genes in Rh*LOL1*-silenced rose plants.

Table S4 Differentially expressed *Aux/IAA* members in Rh*LOL1*-silenced rose plants.

Please note: Wiley is not responsible for the content or functionality of any Supporting Information supplied by the authors. Any queries (other than missing material) should be directed to the *New Phytologist* Central Office.